Radiation Laboratory Technical Report RL-XXXX
Final Report of NASA NNG05GB80G
The University of Michigan Project/Grant F011937

A MODEL-BASED MICROWAVE BRIGHTNESS ALGORITHM FOR ESTIMATING SNOW WETNESS

A. W. England
Department of Electrical Engineering and Computer Science and
Department of Atmospheric, Oceanic, and Space Sciences
University of Michigan

9 November 2007

Abstract

The Pendular Ring Radiobrightness (PRR) Model has been developed to predict the microwave brightness temperature of a wet snowpack. The profiles needed to characterize a wet snowpack are snow density with depth, liquid water content with depth, and average grain size with depth. These can be obtained from snow pit observations, or from models such as SNTHERM or our improved version of SNTHERM, the Snow-Soil-Vegetation-Atmosphere Transfer (SSVAT) Model, which includes liquid water and water vapor exchanges between snow and soil. Comparisons between observed and predicted brightness for the 2003 Cold Lands Processes Experiment (CLPX'03) near Fraser, CO, verify that the PRR Model predictions for the 6.7 and 19 GHz brightness adequately track the observations, and that the fit is incrementally better in most cases when the SSVAT Model is substituted for the SNTHERM Model.

This Report is a compilation of two documents about work done under this grant: I. Chapter 4 of Yi-Ching Chung's PhD dissertation, and II. The paper, "A Pendular Ring Model for Microwave Emission from a Moist Snow Pack" by R.D. DeRoo, A.W. England, Y.-C. Chung, E. Weininger, and K.M. Howell, a version of which will be submitted to Radio Science for publication.

I. PENDULAR RING RADIOBRIGHTNESS MODEL FOR WET SNOW

Y.-C. Cung, from the dissertation entitled, A Snow-Soil-Vegetation-Atmosphere Transfer/Radiobrightness Model for Wet Snow, submitted in partial fulfillment of the requirements for the degree of Doctor of Philosophy, University of Michigan, 2007.

4.1 Introduction of Pendular Ring

The pendular ring radiobrightness model is developed for a wet snowpack. Liquid water in the snowpack accumulates at the contact points between snow particles, forming pendular rings. A wet snowpack will remain stable at low saturation levels (< 7%). Because pendular rings are the natural form of liquid water in a wet snowpack at liquid saturation levels, it is important to characterize the absorption of these rings. Fig 4.1 presents a drawing of this arrangement and offers an ideal representation of the cross section of a single pendular ring of water between two ice particles (Barlow, 2002). As water accumulates in the snowpack, the volume of each ring increases while maintaining the pendular ring formation. This pendular ring concept will be the basis for absorption and scattering in the moist snow pack radiobrightness module.

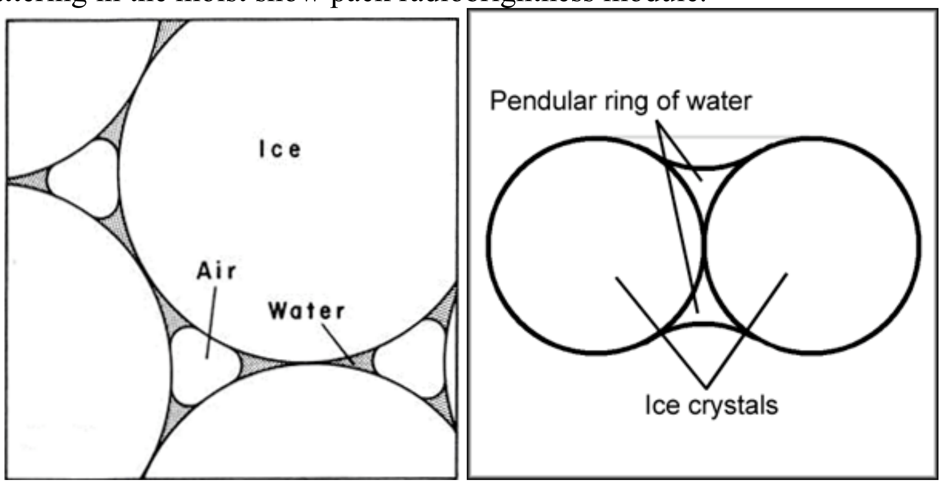

Figure 4.1(a): Pendular ring in wet snow; (b): A pendular ring of water (Barlow, 2002).

4.2 Volume of Pendular Rings and Number Density

Shown as in Fig 4.2, the volume of the pendular ring and number density are calculated when two spheres in contact. The contact angle between the solid surface and the fluid-fluid interface is not zero (Gvirtzman and Roberts, 1991).

$$V_p = 2\pi a^3\{(1-\cos\phi)^2[1-\cot\gamma\cdot[\sin\phi+\cot\gamma(1-\cos\phi-(\frac{\sin\phi}{\cos\gamma}+\frac{1-\cos\phi}{\sin\gamma})\frac{\gamma}{\cos\gamma})]]\} \tag{4.1}$$

where V_p is the pendular ring volume [m^3]; a is the snow grain radius [m]; ϕ is the half-filling angle; γ is the liquid-solid contact angle.

The number of pendular rings depends on the number of spheres which each sphere touches. A unit cell contains $n/2$ complete pendular rings, as each pendular ring belongs to two neighboring spheres and its volume is $8R^3$. The number density, N, of the pendular rings can be computed from the geometry as:

$$N = \frac{n/2}{\frac{4}{3}\pi R^3\left(\frac{1}{1-\varepsilon}\right)} = \frac{3n(1-\varepsilon)}{8\pi R^3} \tag{4.2}$$

where ε is the porosity [-]; n =6 is the number of pendular ring in a unit cell for cubic packing and R is the radius of the ice spheres [m].

The pendular ring volume to whole medium can be extrapolated as:

$$V = N \cdot V_P \tag{4.3}$$

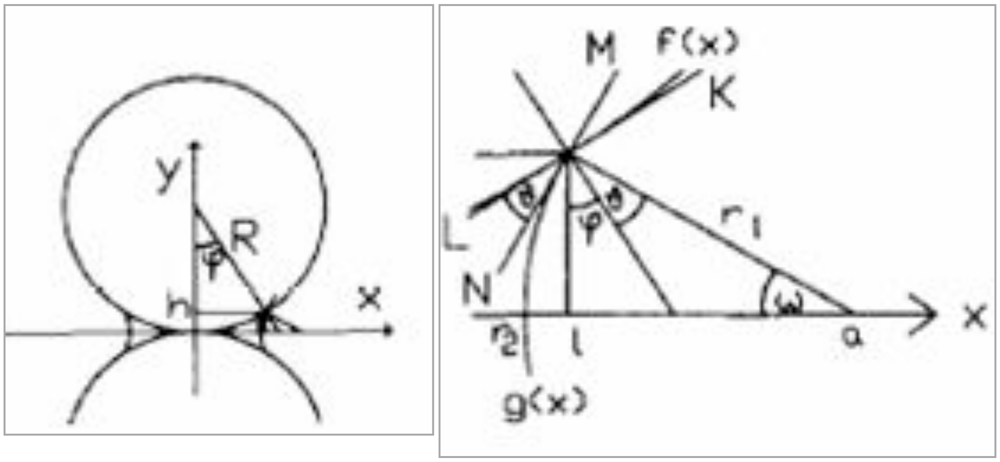

Figure 4.2: Cross sections through pendular ring without/with soil-liquid contact angle (Fig 4b in Gvirtzman and Roberts, 1991).

4.3 Scattered Electromagnetic Fields

The scattered far-field radiation from a pendular ring of liquid water can be found in Rayleigh approximation and the absorption cross section is obtained from the forward scattering theorem of the pendular ring. Rayleigh scattering can be assumed because the size of the pendular ring is much smaller than the microwave wavelength. In the far-field, the Rayleigh scattered fields for a non-magnetic dielectric are expressed as (Kleinman and Senior, 1986):

$$\begin{aligned} E^s(r) &= \frac{e^{ikr}}{4\pi r} S(\hat{r}, \hat{k}, \hat{a}) \\ H^s(r) &= \frac{1}{\eta} E^s(r) \end{aligned} \tag{4.4}$$

$$S(\hat{r}) = -k^2 \{ [\hat{r} \times (X(\varepsilon_r)) \bullet \hat{a}] + [\hat{r} \times (X(\mu_r)) \bullet \hat{b}] + O(k^3) \} \tag{4.5}$$

where $S(\hat{r})$ is the scattering coefficient; k is the wave number in the medium [m^{-1}]; $\hat{r}$ is the unit vector in the observed direction; $\hat{k}$ is the unit vector in the incident wave direction; $\hat{a}$ is the unit vector in the electric field (polarization) direction; $\hat{b}$ is the unit vector in the magnetic field direction; η is the intrinsic impedance of the medium [Ω];

$X(\varepsilon_r)$ is the electrostatic polarizability tensor; $X(\mu_r)$ is the magnetostatic polarizability tensor.

Because the water particle is non-magnetic, there is no magnetic dipole moment. The scattering coefficient reduces to:

$$S(\hat{r}) = -k^2\{\hat{r}\times[\hat{r}\times(X(\varepsilon_r))\bullet\hat{a}]\} \tag{4.6}$$

$X(\varepsilon_r)$ depends on the geometry and the relative permittivity of the dielectric and is found by solving for the electrostatic potential within the pendular ring. The electrostatic polarizability tensor can be simplified based on the geometry of the dielectric scatterer when the dielectric exhibits axial symmetry (Kleinman, and Senior, 1986). When the dielectric exhibits axial symmetry, $X(\varepsilon_r)$ reduces to:

$$X(\varepsilon_r) = \begin{bmatrix} P_{11} & 0 & 0 \\ 0 & P_{11} & 0 \\ 0 & 0 & P_{33} \end{bmatrix} \qquad P_{ii} = 4(1-\varepsilon)\int_{B_{++}} \hat{n}\bullet\hat{x}_i\Phi_i^t dS \tag{4.7}$$

where Φ_i^t is the total electrostatic potential; i=1,2,3 are Cartesian coordinates; $\hat{n}$ is outward unit vector normal to the dielectric body B; B_{++} is the portion of the surface of the dielectric where $x_1, x_2 \geq 0$. P_{11}, P_{33} can be obtained from the program DIELCOM (Senior and Willis, 1982)

4.4 Absorption Coefficient

The module of absorption for wet snow has been modified by Etai Weininger and Roger De Roo (Chung et al., 2006) using the program DIELCOM, which finds the electrostatic polarizability tensor of arbitrary bodies-of-rotation and arbitrary dielectric (Senior and Willis, 1982; Kleinman and Senior, 1986).

The differential scattering cross section is the ratio of scattered to incident power, given by (Kleinman and Senior, 1986):

$$\sigma(\hat{r}) = \frac{1}{4\pi}\left|S(\hat{r},\hat{k},\hat{a})\right|^2 \tag{4.8}$$

It is assumed that the pendular rings are distributed uniformly in a wet snowpack. The scattering cross section of a single ring can be found be averaging the scattering cross section over all possible ring orientations. The rotated polarizability tensor becomes:

$$X'(\varepsilon_r) = R \bullet X(\varepsilon_r) \bullet R^T$$
$$R = \begin{bmatrix} \cos\phi_r & \cos\theta_r \sin\phi_r & \sin\theta_r \sin\phi_r \\ -\sin\phi_r & \cos\theta_r \cos\phi_r & \sin\theta_r \cos\phi_r \\ 0 & -\sin\phi_r & \cos\phi_r \end{bmatrix} \tag{4.9}$$

The total scattering cross section can then be found through integrating the differential scattering cross section over all directions:

$$\sigma_{s,pw} = \frac{k^4}{18\pi}\left(2|P_{11}|^2 + |P_{33}|^2\right) \tag{4.10}$$

The extinction cross section is defined as (Kleinman and Senior, 1986):

$$\sigma_{e,pw} = \frac{1}{k}\operatorname{Im}\left\{S\left(\hat{k},\hat{k},\hat{a}\right)\right\} \tag{4.11}$$

The extinction cross section can be integrated over 4π steradians to obtain (Kleinman, and Senior, 1986):

$$\sigma_{e,pw} = -\frac{k}{3}\operatorname{Im}(2P_{11} + P_{33}) \tag{4.12}$$

The extinction coefficient is the sum of the absorption cross section and scattering cross section:

$$\sigma_{a,pw} = \sigma_{e,pw} - \sigma_{s,pw} \tag{4.13}$$

So the absorption cross section of a pendular ring $\sigma_{a,pw}$ becomes:

$$\sigma_{a,pw} = -\frac{k}{3}\operatorname{Im}\{2P_{11} + P_{33}\} - \frac{k^4}{18\pi}\left(2|P_{11}|^2 + |P_{33}|^2\right) \tag{4.14}$$

The results are the same for horizontal and vertical polarization. This is expected since the equations are integrated over all possible orientations of the pendular ring.

The absorption cross section of the pendular ring is compared with those of a liquid water sphere of equal volume as a metric for the absorption efficiency of the pendular ring in Chapter 4. The absorption cross section for a sphere $\sigma_{a,sw}$ in the Rayleigh approximation is by (Ulaby et al., 1981):

$$\sigma_{a,sw} = -4\pi ka^3 \operatorname{Im}\left\{\frac{\varepsilon_r - 1}{\varepsilon_r + 2}\right\}, \tag{4.15}$$

and the absorption coefficient for spheres of liquid water [NP/m] is:

$$\kappa_{a,pw} = N \cdot \sigma_{a,pw} \tag{4.16}$$

In addition to the component of scatterers (water pendular ring), the total absorption coefficient must include the contribution of the medium (ice particles).

$$\kappa_{a,t} = N \cdot \sigma_{a,pw} + \kappa_{a,i} \tag{4.17}$$

$$\kappa_{a,i} = 2k_0 \cdot n''_{r,i} \tag{4.18}$$

where $k_0 = 2\pi/\lambda_0$ is the wave number in free space [m^{-1}]; $n''_{r,i}$ is the imaginary part of the refractive index of ice [-].

4.5 Dielectric Properties

Pendular ring not only influences the imaginary part of dielectric constant (absorption) of water pendular ring but also influences the real part of the dielectric constant of these rings. So the dialectic constant can be derived as:

$$\begin{aligned} n &= n + j\kappa \\ &= n_b\left[1 + \frac{N}{6}\left(2P_{11} + P_{33}\right)\right] \end{aligned} \tag{4.19}$$

Propagation properties of wet snow are different from those of dry snow. The dielectric constant of snow is given by:

$$\varepsilon_{snow} = n\varepsilon_i + \theta_w \varepsilon_w + \theta_a \varepsilon_a \tag{4.20}$$

where $\varepsilon_i = 3.15$ for ice; $\varepsilon_a = 1$ for air; $\varepsilon_w = \varepsilon_\infty + \dfrac{(\varepsilon_0 - \varepsilon_\infty)}{1 + j\frac{f}{f_0}}$ for liquid water.

$f_0 = \dfrac{1}{1.1109 \cdot 10^{-10}}$ and $\varepsilon_0 = 88.045$ (Ulaby et al., 1986).

The complex dielectric constant of wet soil can be approximated with a mixing model as (Dobson et al., 1985; Ulaby et al., 1986; Liou, 1996):

$$\varepsilon_{soil}^{\alpha} = \theta_{soil,ddry}\varepsilon_{soil,dry}^{\alpha} + \theta_a \varepsilon_a^{\alpha} + \theta_{fw}\varepsilon_{fw}^{\alpha} + +\theta_{bw}\varepsilon_{bw}^{\alpha} + \theta_i \varepsilon_i^{\alpha} \tag{4.21}$$

where $\varepsilon_{soil,dry}, \varepsilon_a, \varepsilon_{fw}, \varepsilon_{bw}, \varepsilon_i$ are dielectric constant of dry soil, air, free water, bound water and ice, respectively, $\varepsilon_{soil,dry} = (1.01 + 0.00044\rho_{soil})^2 - 0.062$; $\varepsilon_{bw} = 31 + j15$ (Dobson et al., 1985); $\alpha = 0.65$ (Dobson et al., 1985); $\theta_{soil,dry}, \theta_a, \theta_{fw}, \theta_{bw}, \theta_i$ represents the volumetric fraction of dry soil, air, free water, bound water and ice, respectively [m^3/m^3], $\theta_{bw} = 0.035$ (Liou, 1996);

4.6 Radiative Transfer Model

The Radiative Transfer Equation (RTE) relates the emitted temperature brightness of a snowpack to the kinetic temperature of the snowpack as well as the absorption and scattering of microwave energy from particles in the snowpack. In this study, the RTE without scattering was used because absorption dominates for wet snow at the lower microwave frequencies. The RTE states as (Ulaby et al., 1981):

$$\mu \frac{dT_{bp}(z,\mu)}{dz} + \kappa_{a,t}(z) T_{bp}(z,\mu) = \kappa_{a,t}(z) T(z) \tag{4.22}$$

where $T_{bp}(z,\mu)$ is the emitted polarized brightness temperature [K]; $\mu = \cos\theta$, θ is incidence angle [rad]; $T(z)$ is physical temperature [K].

The method of invariant embedding is applied for the inhomogeneous snow profiles as shown following equation and in Fig 4.3 (Tsang et al., 1985).

$$\begin{aligned}
[T_{b,0}]_{2\times 1} &= [B_{0,h}]_{2\times 2}[T_{b,h}]_{2\times 1} + (BS)_{2\times N}(T)_{N\pm\times 1} \\
\begin{bmatrix} T_{b,0}^{+} \\ T_{b,sky} \end{bmatrix} &= \begin{bmatrix} B_{11} & B_{12} \\ B_{21} & B_{22} \end{bmatrix} \begin{bmatrix} T_{b,h}^{+} \\ T_{b,h}^{-} \end{bmatrix} + \begin{bmatrix} C_1 \\ C_2 \end{bmatrix} \\
[B_{0,h}]_{2\times 2} &= B_{0,1} \cdot B_{1,2} \cdot \ldots\ldots\ldots B_{N,h} \\
(BS)_{2\times N} &= \{S_{0,1} \quad B_{0,1}S_{1,2} \quad \ldots\ldots \quad B_{0,N-1}S_{N-1,N}\}
\end{aligned} \tag{4.23}$$

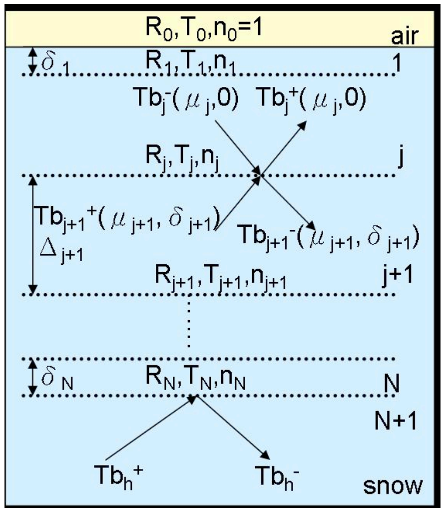

Figure 4.3: Diagram for Invariant Embedding.

4.7 Contribution of Trees

The apparent radiobrightness of snow in the open includes not only the graybody emission from snow in front of the antenna, but also possible emissions from surrounding trees. The contribution of tree on the downwelling brightness temperature should be considered when a small clearing is adjacent to tall trees. The amount of downwelling brightness from these trees on the snowpack can be represented as (De Roo et al., 2006):

$$T_{b,st}^{\downarrow} = \frac{T_{b,sky}(\theta)\Omega_{r,sky}(\theta) + e_{tree}T_{tree}\Omega_{r,tree}(\theta)}{\Omega_{r,sky}(\theta) + \Omega_{r,tree}(\theta)}$$

where $T_{b,sky}$ is the sky brightness temperature [K] at θ, which can be calculated from air temperature, surface pressure and relative humidity (Ulaby et al., 1981); T_{tree} is the physical temperature of trees [K], which can be treated as air temperature; e_{tree} is the emissivity of the tree [-]; and $\Omega_{r,sky}$ $\Omega_{r,sky}$ are the solid angle of sky and trees [sr], which are calculated using the fisheye photo and Gaussian antenna pattern (De Roo et al., 2006).

It is assumed that trees are isotropic emitters. The approximation of physical temperature as air temperature is made because the surface area of the trees is very high compared to its volume. The superimposing Gaussian approximation is used on the microwave antenna gain pattern of the individual radiometer to get the partition of the main beams filled with trees and with sky. This Gaussian distribution model is more accurate to simulate a circular beam pattern than a circle model is. A fisheye photograph is used to estimate the solid angles of sky and trees from background. This downwelling brightness is incorporated in the invariant embedding algorithm instead of sky brightness temperature used before (De Roo et al., 2006).

VIII References

1) Chang, A.T.C., Foster, J.L., Hall, D.K., Rango, A., Hartline, B.K., 1982, Snow water equivalent estimation by microwave radiometry, *Cold Regions Science and Technology, v. 5*, no. 3, pp. 259-267.

2) Goodison, B.E.; Walker, A.E.; Thirkettle, F.W.; et al, 1990, Determination of snow water equivalent on the Canadian prairies using near real-time passive microwave data, Ed. Kite, G.W., Wankiewicz, A., *Workshop on Applications of Remote Sensing in Hydrology*, Saskatoon, Saskatchewan, Feb. 13-14, pp. 297-316.

3) England, A.W., 1974, Thermal microwave emission from a halfspace containing scatterers, *Radio Science, 9*, pp. 447-454.

4) England, A.W., 1975, Thermal microwave emission from a scattering layer, J. *Geophysical Research, 80*, pp. 4484-4496.

5) Jordan, R., 1991, A one-dimensional temperature model for a snow cover, Technical documentation for SNTHERM.89, *Special Technical Report 91-16*, US Army CRREL, Hanover, N.H.

6) Denoth, A., 1982, The pendular-funicular liquid transition and snow metamorphism, *J. Glaciology, 28*, pp. 357-364.

7) Kleinman, R.E., and Senior, T.B.A., 1986, Rayleigh scattering, Chap. 1 in, *Low and High Frequency Asymptotics*, V.K. Varadan and V.V. Varadan, Eds., Elsevier.

II. A Pendular Ring Model for Microwave Emission from a Moist Snow Pack (paper attached)

Radio Science, Volume ???, Number , Pages 1–19,

A Pendular Ring Model for Microwave Emission from a Moist Snow Pack

R. D. De Roo,[1] A. W. England,[1,2] Y.-C. Chung,[1] E. Weininger,[3] and K. M. Howell[4]

R. D. De Roo, Department of Atmospheric, Oceanic, and Space Sciences, University of Michigan, Ann Arbor, MI 48109, USA. (deroo@umich.edu)

[1]Department of Atmospheric, Oceanic, and Space Sciences, University of Michigan, Ann Arbor, MI, USA.

[2]Department of Electrical Engineering and Computer Science, University of Michigan, Ann Arbor, MI, USA.

[3]NASA Jet Propulsion Laboratory, Pasedena, CA, USA.

[4]Davidson College, Davidson, NC, USA.

A pendular ring model for the microwave emission from the liquid water in a snow pack is introduced. In snow that has metamorphosed, the ice particles tend towards a spherical shape and the liquid water collects first at the contact points between ice grains. At these contact points, while the liquid moisture content remains below about 7% by volume, the water forms rings as a result of capillary action. The impact of this ring geometry on the static dielectric properties of the water is analyzed. The electromagnetic losses in a snow pack due to the presence of these rings is significantly higher than if the same volume of water in each ring were considered to be a spherical droplet.

1. Introduction

The radio brightness of snow packs are routinely used to predict snow pack properties such as snow depth and snow water equivalent (SWE) from space (Chang *et al.* [1997]; Derksen *et al.* [2005]; Guo *et al.* [2003]; Kelly *et al.* [2003]; Wilson *et al.* [1999]). Radio frequency observations are preferred because optical remote sensing techniques to quantify these snow parameters saturate at snow pack depths on the order of 5 cm (Baker *et al.* [1991]). In the microwave region, the extinction of dry snow has a sharp spectral gradient (Hallikainen *et al.* [1987]), permitting dual frequency measurements to differentiate parameters of the snow pack from other sources of emission (such as the ground, or the atmosphere). The emission from a snow pack, however, is very sensitive to many parameters, including not only density and depth, but also snow grain size, snow grain shape, and correlations in the positions of snow grains. This sensitivity to the microscopic features of the snow pack are related to the fact that snow grain sizes are comparable in size to typical microwave wavelengths. Unfortunately, because these snow grains are very densely packed, interactions amongst these grains leads to very complex scattering of microwaves within the snow pack. Despite increasingly sophisticated efforts to model the electromagnetic behavior of snow, from simple radiative transfer techniques (Kuga *et al.* [1991]), to dense media techniques incorporating multiple scattering (Tsang and Kong [1992]; Tsang *et al.* [2007]), the only operational algorithms using microwave observations of snow to extract parameter estimates are heuristic. These heuristic microwave algorithms are restricted to the condition of dry snow only, as snow with any amount of liquid moisture appears to be much brighter (Arslan *et al.* [2005]; Ashcraft and Long [2005]) than dry snow. This is because the dielectric constant and especially the loss factor of liquid water is much higher than that of ice (Tiuri *et al.* [1984]; Hallikainen *et al.* [1986]; Ulaby *et al.* [1986]) . However, even when restricted to dry snow, the heuristic algorithms do not correctly capture all the subtleties of the snow pack. For example, the perhaps most common technique of relating the difference of the brightness at 19GHz and 37GHz to snow parameters has the following limitations: the addition of very fine grain new snow to the top of the snow pack may decrease the SWE estimate, and grain growth results in predictions of a snow depth increase when, in fact, grain growth leads to a decrease in snow depth (Markus *et al.* [2006]).

In addition to "wet" and "dry" as two distinct states of snow for microwave observations, the wet state can be further distinguished as "pendular" or "funicular" (Ulaby *et al.* [1986]). In the pendular regime (just above 0% to approximately 7% moisture by volume), the moisture collects at the contact points between snow grains, while in the funicular regime (>7%) the moisture coats all surfaces of the grains. The modeling efforts that include liquid water in the snow pack typically treat the moisture as funicular even during low moisture conditions (eg. Macelloni *et al.* [2005]; Tedesco *et al.* [2006]).

In this paper we will analyze the low frequency behavior of snow in the pendular regime, with the snow grains modelled as spheres and the liquid water forming "pendular rings" about the contact points between the snow grains. The approximation of the snow grains as spherical is justified by the fact that when snow begins to melt, the smaller particles melt first and the larger particles accumulate ice in a roughly spherical shape (Male [1980]).

2. Pendular Ring Shape

For two small spheres of ice of equal size which are touching at a single point, water which collects on the surface of the spheres will migrate to the contact point as surface tension minimizes the energy of the configuration of the water body. The shape of the air-water boundary also takes a circular cross section (resembling a portion of a torus) as an additional manifestation of the capillary forces minimizing the energy of the shape of the ring of water. This geometry has been described in detail by Gvirtzman and Roberts [1991] and is shown in cross section in Figure 1. Following their approach, we obtain the volume of the ring, V_p, as

$$V_p = 2\pi R^3 (1 - \cos\phi)^2 \left[1 - \csc^3\omega\,(\cos\omega - \sin\theta)\,(\omega - \sin\omega\cos\omega)\right] \quad (1)$$

where R is the ice sphere radius, 2ϕ is the angle of wetting of the surface of the sphere, $\theta = 24.2°$ is the contact angle within the water at the junction of water, ice and air (van Oss *et al.* [1992]), and $\omega = \pi/2 - \phi - \theta$ is the half angle of the air-water interface.

Assuming that the particles in a dry snow pack are uniformly sized spheres of ice, the volumetric moisture content of the snow pack can be related to the volume of the rings as follows. The number density of ice particles, n_s, in the snow pack is given by

$$n_s = \frac{v_i}{V_s} \quad (2)$$

where v_i is the volume fraction of ice and $V_s = \frac{4}{3}\pi R^3$ is the ice sphere volume. The number density of pendular rings of water, n_w, in the snow pack is given by

$$n_w = n_s \frac{N}{2} \quad (3)$$

where N is the coordination number, that is, the number of rings that touch each sphere. The coordination number is halved because each pendular ring touches two ice particles. The volume fraction of liquid water in the snow pack, v_w, is then

$$v_w = n_w V_p \quad (4)$$

Snow is composed only of ice, liquid water, and air, thus: $v_i + v_w + v_a = 1$, where v_a is the volume fraction of air in the snow pack. The volume fraction of ice in a dry snow pack ($v_w = 0$) is easily derived from snow density measurements: $\rho_{snow} = \rho_i v_i + \rho_a v_a \approx \rho_i v_i$, where ρ_{snow} is the snow density and $\rho_i = 917\text{kg/m}^3$ is the density of ice. The density of air is negligible at $\rho_a = 1.2\text{kg/m}^3$. The common range of snow density is from 100kg/m^3, typical for new snow, to 500kg/m^3 for a metamorphic snow pack.

Because both V_p and V_s are proportional to R^3, the liquid moisture content of a snow pack of uniformly sized spherical ice pellets is a function only of the dry snow density v_i, the coordination number N, and the wetting angle ϕ. Moreover, the coordination number depends on the packing density, that is, on the dry snow density.

Herminghaus [2005] reviewed the techniques for analysis of wet soils, with an application to understanding landslides. We can use similar techniques for metamorphic snow packs. His review of the dependence of the coordination number on packing density reveals a coordination number near $N = 6$ for sphere packing factors near the random close pack density ($v_i \approx 0.64$). For a random packing of glass spheres with a 10% to 20% size distribution, the coordination number ranged from $N = 5.1$ for $v_i = 0.57$ to $N = 5.9$ for $v_i = 0.62$. The number of pendular rings in a random packing is slightly larger than N due to spheres which nearly contact each other.

These values for N are significantly lower than would be found in a crystal structure. For a face centered cubic crystal or a hexagonal close pack crystal, which have a maximum packing density of $v_i = \pi/3\sqrt{2} = 0.74$, the coordination number is $N = 12$. At the other extreme, a loose pack of uniformly sized spheres which can move under gravity must have a coordination number of $N \geq 4$. Barlow [2002] investigated the packing density of infinitely sticky spheres, and the resulting $N \approx 2.3$. Thus, a coordination number of $N \approx 6$ (including both actual and near contact points between spheres) appears to be an appropriate value for a dense, metamorphic snow pack composed of sticky spherical ice grains.

With this value for the coordination number, we can investigate the range of volumetric moisture for which pendular rings can form. For three spheres of uniform size mutually touching each other, the pendular rings must have wetting angles $\phi < 30°$ lest the rings contact each other. Thus, the pendular ring regime of moist snow extends up to $v_w = 6.3\%$. A pendular ring cannot exceed a size at which the capillary forces are insufficient to make the pendular ring shape a minimum energy state. The capillary pressure, P_c, at the interface between the air and water is given by the

Laplace equation (Gvirtzman and Roberts [1991]):

$$P_c = \gamma \left(\frac{1}{r_2} - \frac{1}{r_1} \right) \cos\theta \tag{5}$$

where γ is the surface tension of the water. The minus sign arises from the fact that r_1 and r_2 are defined from opposite sides of the air-water interface in Fig. 1. The condition for zero capillary pressure, $r_1 = r_2$, can be solved to determine an upper bound for the wetting angle, denoted ϕ_{max}, as a function of θ:

$$\phi_{max} = 2\tan^{-1}\left(\frac{\cos\theta}{2+\sin\theta} \right) \tag{6}$$

For $\theta = 24.2°$, we obtain $\phi_{max} = 41.5°$. For metamorphic snow densities of $v_i \leq 600\mathrm{kg/m^3}$ with $N \leq 6$, this results in an upper bound for pendular ring volumetric moisture of $v_w \leq 10\%$. These bounds agree with the 7% value often given for the volumetric moisture of the transition from pendular to funicular (cite???).

3. Pendular Ring Electrical Characteristics

Determining the general scattering and absorption cross sections of a pendular ring of water embedded in a dense random matrix of ice spheres, air, and other pendular rings of water is challenging. To simplify the situation so that we may obtain insights to the physical consequences of the ring shape, we will assume a sufficiently low frequency such that the Rayleigh approximation can apply, and that the interactions between an individual ring and other components of the snow pack, including other rings, can be neglected.

Senior and Willis [1982] introduced DIELCOM, a small computer code for calculating the Rayleigh polarizability tensor of a dielectric body of revolution for which the contour is composed of a finite number of circular arcs and straight lines. We used this computer code to compare the absorption and scattering cross sections of various shapes of the moisture content within the snow pack which are candidates for inclusion in snow emission and scattering models. The shapes we considered are:

1. pendular rings, as described in the previous section,
2. spherical droplets of the same volume as the pendular rings,
3. films of water around each ice particle,
4. spherical droplets of the same volume as the films.

The spherical droplets are considered because the scattering and absoption characteristics are well known, and are therefore easy to implement in complex models (even if none use them now). The films are considered because this configuration for the liquid water in a snow pack has been used in the published literature (eg. Tedesco *et al.* [2006]).

The dielectric value of the DIELCOM shape is the complex ratio of the dielectric value of the water at 0°C to the dielectric of the background, which is a composition of ice and air. We assumed a refractive index mixing model for the constituative materials:

$$\epsilon_{shape}\left(f\right) = \frac{\epsilon_w\left(f, T = 0°\mathrm{C}\right)}{\epsilon_{bkgnd}} = \frac{\epsilon_w(f, T = 0°\mathrm{C})}{\left(\frac{v_i\sqrt{\epsilon_i}+v_a\sqrt{\epsilon_a}}{v_i+v_a}\right)^2} \tag{7}$$

where $\epsilon_i = 3.15 - j0$ is the dielectric constant of ice, $\epsilon_a = 1 - j0$ is the dielectric constant of air, and $\epsilon_w(f, T)$ is the dielectric constant of fresh water as a function of frequency and temperature as given by Klein and Swift [1977]. To simplify the analysis of the effects of geometry of the water inclusions, we will assume that ϵ_{bkgnd} is constant with respect to changes in the volumetric moisture content of the snow. That is, the reduction in v_i due to melting is matched proportionately with a reduction in v_a due to compaction and water migration. At a snow density of $\rho_s = 500\text{kg/m}^3$, $\epsilon_{bkgnd} = 2.023 - j0$. The resulting dielectric values used are given in Table 1.

The range of validity for the Rayleigh approach is that the radius of the scatterers should be at most $\lambda_b/20$ (Ishimaru [1978]), where λ_b is the wavelength in the background medium. For a largest ice sphere diameter of 1 mm, the Rayleigh approximation should be sufficient for snow up to at least 15 GHz.

The output of DIELCOM are the complex polarizabilities $p_{11} = p_{22}$ (aligned with the x- and y-axes) and p_{33} (aligned with the z-axis). These polarizabilities are normalized to the particle's volume, V_p, and so the output from DIELCOM is independent of the ice sphere radius, R, which serves as an overall scale parameter. The normalized polarizabilities at 1.4 GHz as a function of ϕ is shown in Fig. 2 for the pendular rings.

The pendular ring shape is highly assymmetric, as seen in the values normalized polarizabilities (Fig. 2). We will assume that the random packing of ice particles in the snow pack results in a uniform distribution of pendular ring orientations. From the Optical Theorem, the extinction cross section of the particle is

$$\sigma_{ext} = \frac{kV_p}{3}\Im m\left\{2p_{11} + p_{33}\right\} \tag{8}$$

where $k = 2\pi/\lambda_b$ is the wavenumber in the composite medium of ice and air , and $\Im m\{...\}$ operator retains the imaginary part of its argument. Simlarly, the total scattering cross section is given by

$$\sigma_T \;=\; \frac{k^4 V_p^2}{18\pi}\left(2\left|p_{11}\right|^2 + \left|p_{33}\right|^2\right) \tag{9}$$

As the extinction cross section is the sum of the absorption cross section and the total scattering cross section, the absorption cross section can be found from the difference of the two expressions above. However, in the Rayleigh limit ($k \to 0$), scattering is secondary to absorption, and we will use the extinction cross section as the absorption cross section. This is consistent with the output of DIELCOM, as shown in Fig. 3 for L-band. The extinction cross sections exceed the total scattering cross sections by 10 dB or more.

The absorption coefficient for the snow pack is obtained by multiplying each water particle's absorption cross section by the number density of these particles:

$$\kappa_a \;=\; n_w\sigma_a \approx n_w\sigma_{ext} = \frac{kv_w}{3}\Im m\left\{2p_{11} + p_{33}\right\} \tag{10}$$

The absorption coefficient is proportional to the total water content of the snow pack, through v_w. Through p_{11} and p_{33}, the absorption coefficient is a function of the water particle shape and dielectric properties. While we remain in the region of validity for the Rayleigh assumption, the absorption coefficient is not a function of the size of the water particle. Thus, the absorption coefficient for the snow pack with a distribution of spherical water droplets will be the same regardless of whether the water is distributed in as many droplets as there are ice particles, or in as many droplets as there are contact points between ice particles. For this reason, only one curve exists for the cross sections and the absorption coefficent when the liquid water forms spherical droplets.

4. Spherical Film Electrical Model

DIELCOM computes the polarizabilities by integrating over the contour of physical cross section of the body of revolution. The points at which the kernal of the integration are evaluated must be close together when the contour exhibits sharp corners (as in the pendular ring shape) or two parts of the contour are close to each other (as in the film shape). For the thinner films, corresponding to volumetric moisture less than about 2%, DIELCOM is computationally inefficient due to the large number of function evaluations. Therefore, for the film geometry, we are using the algorithm that appears in Bohren and Huffman [1983] for a coated sphere. The absorption cross section predicted in this manner agrees to with 0.3 dB with that predicted by DIELCOM for $v_w > 2\%$. The absorption characteristics of the films as calculated with this algorithm is not a function of the dielectric constant used for the core material of the coated sphere. That is, the absorption coefficient of the film around the ice sphere is independent of whether the ice has been assigned ϵ_i, or ϵ_{bkgnd} (as must be done using DIELCOM).

5. Results

Figure 4 shows the absorption coefficient as a function of moisture content when the liquid water particles form films around the spherical ice grains, pendular rings between ice grains, and as spherical droplets of water. The presumed shape of the water particles has dramatic influence on the predicted absorption. The spherical droplets, most compact geometry for the water particles, produces a low absorption, while the films, which distributes the liquid water over the largest area, produces the highest absorption. The pendular rings, as a shape with physical extent between that of films and spheres, produce an absorption prediction between the two extremes of other two shapes.

While the polarizability of the pendular rings is very assymmetric, the assumption of a uniform distribution of orientations within the snow pack results in an absorption coefficient which is independent of polarization. However, if this assumption is not valid, and ice grains tend to form contacts with orientations that are not uniformly distributed, either due to gravity, wind, or slope, there may be a significant polarization signature in the snow pack.

6. Conclusions

We have modelled the liquid water particles in moist snow as spherical droplets, as pendular rings between ice grains, and as a film on the ice grains. These shapes were analyzed for their microwave absorption in the Rayleigh regime (roughly up to 15 GHz). These presumed shapes of the liquid water dramatically affects the expected absorption of microwave radiation, with the absorption due to films exceeding that from pendular rings, which in turn exceeds that due to spherical droplets.

A. Appendix

A.1. Derivation of Maximum Wetting Angle

Gvirtzman and Roberts [1991] identify the maximum possible wetting angle, ϕ_{max}, as that which occurs with zero capillary forces. This comes about when the radius of curvature of the ring itself, r_2, is equal to the radius of air-water boundary, r_1. From the geometry in Fig. 1, $r_1 = r_2$ is

$$R\frac{1-\cos\phi_{max}}{\sin\omega_{max}} = R\left(\sin\phi_{max} - \frac{(1-\cos\phi_{max})(1-\cos\omega_{max})}{\sin\omega_{max}}\right) \tag{11}$$

where $\omega_{max} = \frac{\pi}{2} - \theta - \phi_{max}$. Therefore,

$$2(1-\cos\phi_{max}) = \cos\omega_{max} - (\cos\phi_{max}\cos\omega_{max} - \sin\phi_{max}\sin\omega_{max}) \tag{12}$$

$$= (\sin\phi_{max}\cos\theta + \cos\phi_{max}\sin\theta) - \sin\theta \tag{13}$$

$$\frac{\cos\theta}{2+\sin\theta} = \frac{1-\cos\phi_{max}}{\sin\phi_{max}} = \tan(\phi_{max}/2) \tag{14}$$

This result is consistent with Gvirtzman and Robert's underived result that $\phi_{max} = 53.1°$ at $\theta = 0°$ and $\phi_{max} = 37.1°$ at $\theta = 32°$.

A.2. Derivation of Pendular Ring Volume

The formulas for the volume of the pendular ring given in Gvirtzman and Roberts [1991] appears to contain typographical errors. The values calculated with their formula for arbitrary θ do not agree with that calculated by DIELCOM. Also, the values of pendular ring volume calculated per Gvirtzman and Roberts [1991] exceed that of a simple geometric shape given by a cylinder of height $2h$ and radius l, minus two cones each with height h and radius l. This shape circumscribes that of the pendular ring, and so the pendular ring volume must be less than this "rotated bowtie" volume of $\left(2 - \frac{2}{3}\right)\pi l^2 h$. A re-derivation of the pendular ring volume, as outlined in the Appendix of Gvirtzman and Roberts [1991], reveals that their equation (A.14) contains a single sign error. Equation (A.14) of Gvirtzman and Roberts [1991] should read:

$$\begin{aligned} V_p \;=\; & 2\pi R^3 \left(1 - \cos\phi\right)^2 \\ & \times \left(1 + \cot\omega \left[\sin\phi + \cot\omega \left(1 - \cos\phi - \left(\frac{\sin\phi}{\cos\omega} + \frac{1 - \cos\phi}{\sin\omega}\right)\frac{\omega}{\cos\omega}\right)\right]\right) \end{aligned} \tag{15}$$

Also, equation (A5) in the same appendix, which describes the ice-water contour in the (z, ρ) plane, contains the wrong sign on the square root, although this does not appear to lead to the sign error in (A14). Equation (A5) of Gvirtzman and Roberts [1991] should read:

$$f(x) = y \;=\; R - \sqrt{R^2 - x^2} \tag{16}$$

Similarly, in equation (A9), the sole appearance of r_1 should be squared. Finally, the result for the volume of a pendular ring when $\theta = 0°$, given in equation (A10), also is not correct as printed. As this is a special case of (A14), the above formula should be used instead.

References

Arslan, A. N., M. T. Hallikainen, and J. T. Pullianen, 2005, IEEE Transactions on Geoscience and Remote Sensing **43**(8), 1827.

Ashcraft, I. S., and D. G. Long, 2005, IEEE Transactions on Geoscience and Remote Sensing **43**(6), 1317.

Baker, D. G., R. H. Skaggs, and D. L. Ruschy, 1991, Journal of Applied Meteorology **30**, 387.

Barlow, J., 2002, *Mathematical Modelling of Snow*, PhD dissertation, University of Bristol, Bristol, England.

Bohren, C. F., and D. R. Huffman, 1983, *Absorption and Scattering of Light by Small Particles* (Wiley-Interscience, New York).

Chang, A. T. C., J. L. Foster, D. K. Hall, B. E. Goodison, A. E. Walker, J. R. Metcalfe, and A. Harby, 1997, Journal of Geophysical Research **102**(D24), 29,663.

Derksen, C., A. E. Walker, B. E. Goodison, and J. W. Strapp, 2005, IEEE Transactions on Geoscience and Remote Sensing **43**(5), 960.

Guo, J., L. Tsang, E. G. Josberger, A. W. Wood, J.-N. Hwang, and D. P. Lettenmaier, 2003, IEEE Transactions on Geoscience and Remote Sensing **41**(3), 612.

Gvirtzman, H., and P. V. Roberts, 1991, Water Resources Research **27**(6), 1165.

Hallikainen, M. T., F. T. Ulaby, and M. Abdelrazik, 1986, IEEE Transactions on Antennas and Propagation **34**(11), 1329.

Hallikainen, M. T., F. T. Ulaby, and T. E. van Deventer, 1987, IEEE Transactions on Geoscience and Remote Sensing **25**(6), 737.

Herminghaus, S., 2005, Advances in Physics **54**(3), 221.

Ishimaru, A., 1978, *Wave Propagation and Scattering in Random Media*, volume 2 (Academic Press, New York).

Kelly, R. E., A. T. Chang, L. Tsang, and J. L. Foster, 2003, IEEE Transactions on Geoscience and Remote Sensing **41**(2), 230.

Klein, L. A., and C. T. Swift, 1977, IEEE Transactions on Antennas and Propagation **25**(1), 104.

Kuga, Y., F. T. Ulaby, T. F. Haddock, and R. D. De Roo, 1991, Radio Science **26**(2), 329.

Macelloni, G., S. Paloscia, P. Pampaloni, M. Brogioni, R. Ranzi, and A. Crepaz, 2005, IEEE Transactions on Geoscience and Remote Sensing **43**(11), 2431.

Male, D. H., 1980, *The Seasonal Snowcover* (Academic Press, New York), chapter 6, pp. 305–395.

Markus, T., D. C. Powell, and J. R. Wang, 2006, IEEE Transactions on Geoscience and Remote Sensing **44**(1), 68.

Senior, T. B. A., and T. M. Willis, III, 1982, IEEE Transactions on Antennas and Propagation **30**(6), 1271.

Tedesco, M., E. J. Kim, A. W. England, R. D. De Roo, and J. P. Hardy, 2006, IEEE Transactions on Geoscience and Remote Sensing **44**(12), 3563.

Tiuri, M. E., A. H. Sihvola, E. G. Nyfors, and M. T. Hallikainen, 1984, IEEE Journal of Oceanic Engineering **9**(5), 377, invited Paper.

Tsang, L., and J. A. Kong, 1992, Journal of Electromagnetic Waves and Applications **6**(8), 256.

Tsang, L., J. Pan, D. Liang, Z. Li, D. W. Cline, and Y. Tan, 2007, IEEE Transactions on Geoscience and Remote Sensing **45**(4), 990.

Ulaby, F. T., R. K. Moore, and A. K. Fung, 1986, *Microwave Remote Sensing: Active and Passive* (Artech House, Norwood, MA), volume 3, appendix E, pp. 2017–2119.

van Oss, C. J., R. F. Giese, R. Wentzek, J. Norris, and E. M. Chuvilin, 1992, Journal of Adhesion Science Technology **6**(4), 503.

Wilson, L., L. Tsang, J.-N. Hwang, and C.-T. Chen, 1999, IEEE Transactions on Geoscience and Remote Sensing **37**(2), 690.

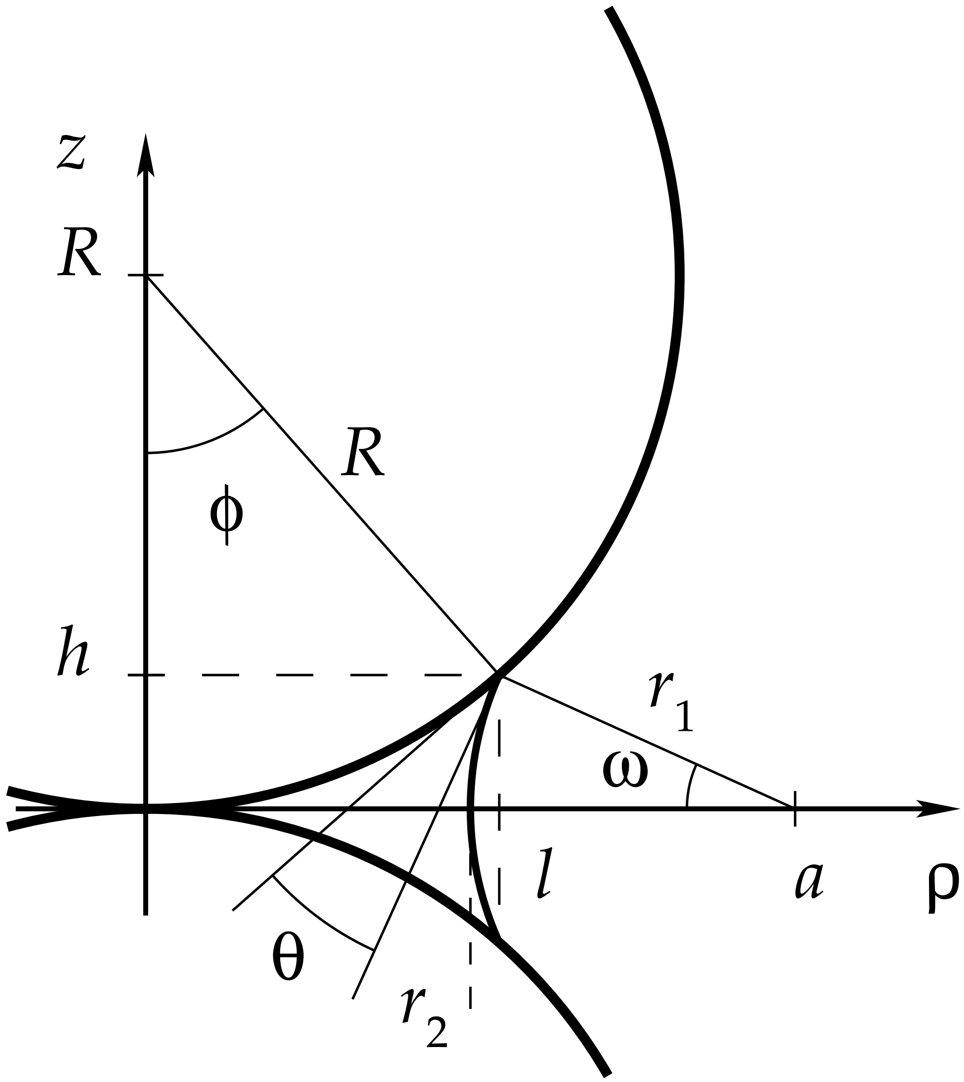

Figure 1. Geometric parameters of a pendular ring. Some of the relationships between parameters include: $\omega = \pi/2 - \theta - \phi$; $h = R(1 - \cos\phi) = r_1 \sin\omega$; $l = R\sin\phi$; $a = r_1 + r_2 = l + r_1 \cos\omega$. In this figure, $\theta = 24.2°$ and $\phi = 41.5°$.

Table 1. Dielectric Values Used in DIELCOM

frequency GHz	ϵ_w at 0°C	ϵ_{shape} at $\rho_s = 500\text{kg/m}^3$
1.4	86.04 -j 12.74	42.53 -j 6.30
6.9	57.27 -j 40.15	28.31 -j 19.85
10.7	39.36 -j 40.96	19.46 -j 20.25
18.7	20.54 -j 32.49	10.15 -j 16.06

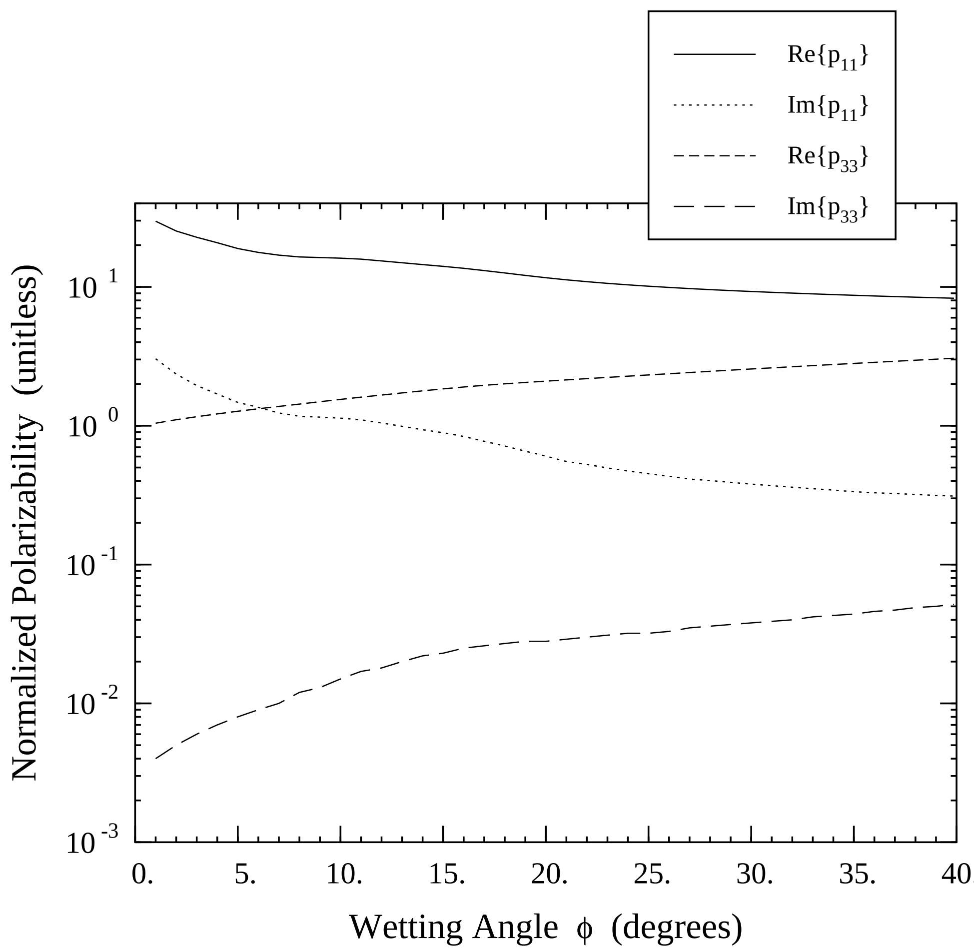

Figure 2. Example DIELCOM output for liquid water in the pendular ring shape. This example is at 1.4 GHz.

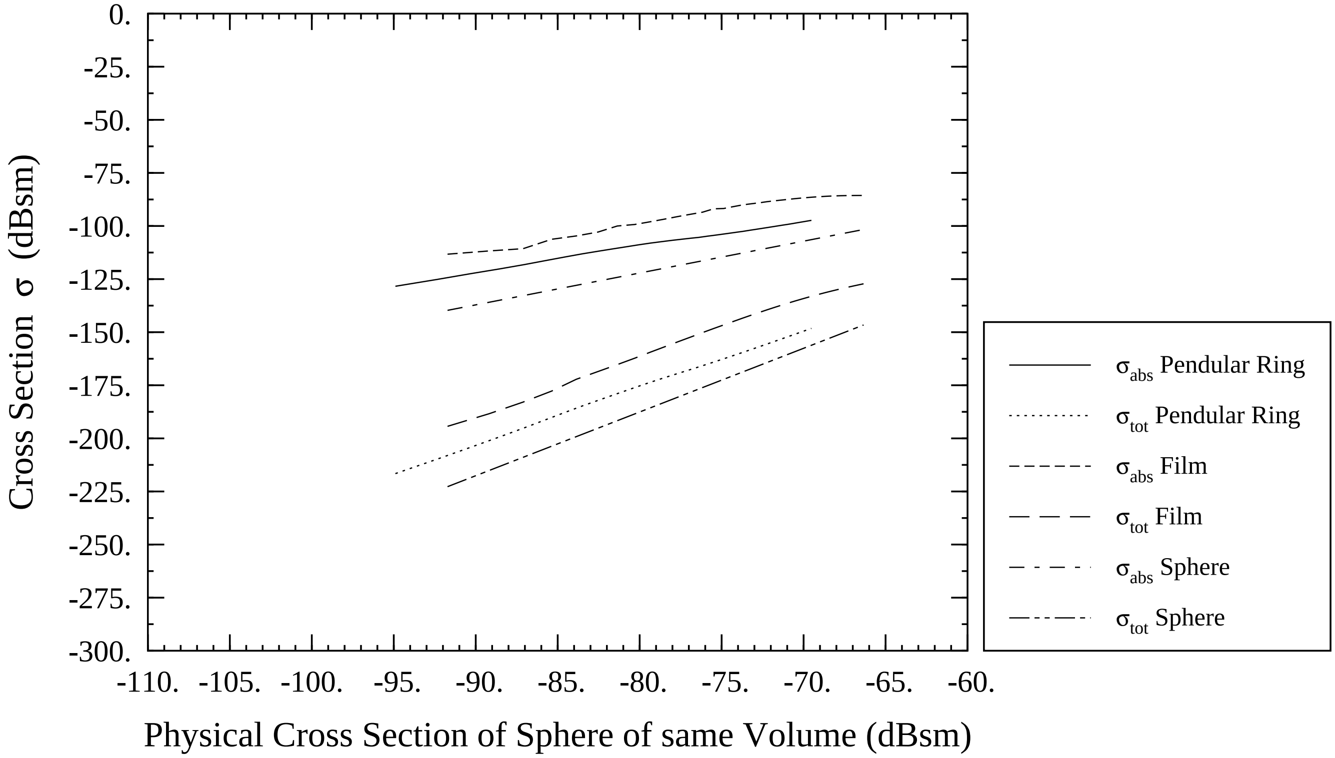

Figure 3. Extinction and scattering cross sections for particles of liquid water of various shapes. The horizontal axis is the size of the water particle in terms of the cross section of a sphere of the same volume. This example is at 1.4 GHz for snow pack with a dry density of 500 kg/m^3 and composed of spherical ice particles 1 mm in diameter.

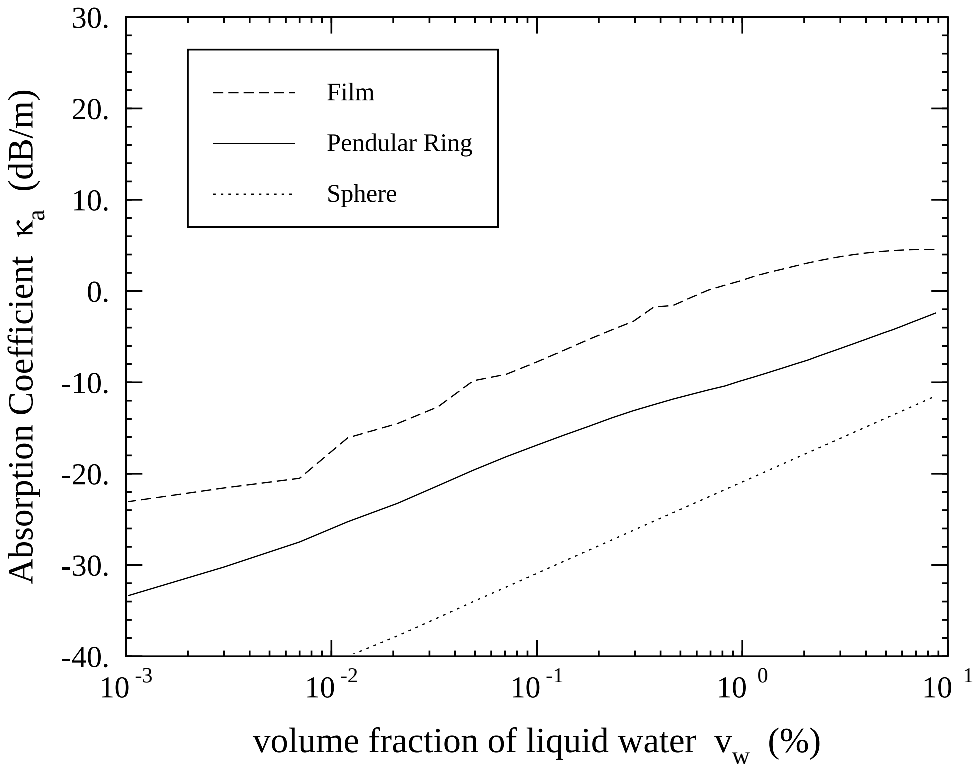

Figure 4. Absorption coefficients of moist snow as a function of moisture content, by presumed shape of the liquid water particles. This example is at 1.4 GHz for snow pack with a dry density of 500 kg/m^3, composed of spherical ice particles 1 mm in diameter, and a coordination number of 6 pendular rings touching each ice sphere.